

APO TIME RESOLVED COLOR PHOTOMETRY OF HIGHLY-ELONGATED INTERSTELLAR OBJECT 1I/'OUMUAMUA

BRYCE T. BOLIN,^{1,2,3} HAROLD A. WEAVER,⁴ YANGA R. FERNANDEZ,⁵ CAREY M. LISSE,⁴ DANIELA HUPPENKOTHEN,¹
R. LYNNE JONES,¹ MARIO JURIC,¹ JOACHIM MOEYENS,^{1,6} CHARLES A. SCHAMBEAU,⁵ COLIN. T. SLATER,¹ ŽELJKO IVEZIĆ,¹
AND ANDREW J. CONNOLLY¹

¹*Department of Astronomy, University of Washington, 3910 15th Ave NE, Seattle, WA 98195*

²*B612 Asteroid Institute and DIRAC Institute Postdoctoral Fellow*

³*Laboratoire Lagrange, Université Côte d'Azur, Observatoire de la Côte d'Azur, CNRS, Blvd. de l'Observatoire, CS 34229, 06304 Nice cedex 4, France*

⁴*Johns Hopkins University Applied Physics Laboratory, Laurel, MD 20723*

⁵*Department of Physics, University of Central Florida, Orlando, FL 32816, USA*

⁶*LSSTC Data Science Fellow*

(Received -; Revised -; Accepted -)

Submitted to ApJL

ABSTRACT

We report on g , r and i band observations of the Interstellar Object 1I/'Oumuamua (1I) taken on 2017 October 29 from 04:28 to 08:40 UTC by the Apache Point Observatory (APO) 3.5m telescope's ARCTIC camera. We find that 1I's colors are $g - r = 0.41 \pm 0.24$ and $r - i = 0.23 \pm 0.25$, consistent with visible spectra (Masiero 2017; Ye et al. 2017; Fitzsimmons et al. 2017) and most comparable to the population of Solar System C/D asteroids, Trojans, or comets. We find no evidence of any cometary activity at a heliocentric distance of 1.46 au, approximately 1.5 months after 1I's closest approach distance to the Sun. Significant brightness variability was seen in the r observations, with the object becoming notably brighter towards the end of the run. By combining our APO photometric time series data with the Discovery Channel Telescope (DCT) data of Knight et al. (2017), taken 20 h later on 2017 October 30, we construct an almost complete light curve with a most probable lightcurve period of $P \simeq 4$ h, and reveal the most useful locations during 1I's rotation phase for additional data to improve constraints on its lightcurve. Our results imply a double peaked rotation period of 8.1 ± 0.02 h, with a peak-to-peak amplitude of 1.5 - 2.1 mags. Assuming that 1I's shape can be approximated by an ellipsoid, the amplitude constraint implies that 1I has an axial ratio of 4.1 to 6.9, which is strikingly elongated. Assuming that 1I is rotating below its critical break up limit, our results are compatible with 1I having a density > 1.0 g cm⁻³, or having modest cohesive strength. Astrometry useful for constraining 1I's orbit was also obtained and published in Weaver et al. (2017).

Keywords: minor planets, asteroids: individual (1I/2017 U1 ('Oumuamua)), galaxy: local interstellar matter

1. INTRODUCTION

The discovery and characterization of protoplanetary disks have provided ample observational evidence that icy comet belts and rocky asteroid belts exist in other planetary systems (*e.g.* Lisse et al. 2007; Öberg et al. 2015; Nomura et al. 2016; Lisse et al. 2017). However, these observations have consisted of distant collections of millions of objects spanning large ranges of temperature, astrocentric distance, and composition. Until now, it has been impossible to bring the level of detailed analysis possible for our own local small body populations to the large, but unresolved, groups of comets and asteroids in exoplanetary disks.

The observation and discovery of interstellar objects have been discussed before (Cook et al. 2016; Engelhardt et al. 2017), but the apparition of 1I/‘Oumuamua (hereafter “1I”) is the first opportunity to study up close an asteroid-like object that formed outside of the Solar System. This provides a unique opportunity to measure the basic properties (size, shape, rotation rate, color) of a small body originating in another planetary system, and compare it directly to the properties of cometary nuclei and asteroids in our own. Such measurements may shed light on how and where 1I formed within its planetary system, as well provide a basis for comparison to potential Solar System analogs.

In this work, we describe APO/ARCTIC imaging photometry in three bands, g , r and i taken to meet three scientific goals: (a) measure the color of the object’s surface, to compare with our own small body populations; (b) perform a deep search for cometary activity in the form of an extended coma; and (c) constrain the object’s rotation period to make an initial assessment of structural integrity.

2. OBSERVATIONS

Photometric imaging observations of 1I were acquired on 2017 October 29 (UTC) using the ARCTIC large format CCD camera (Huehnerhoff et al. 2016) on the Apache Point Observatory’s (APO’s) 3.5m telescope. The camera was used in full frame, quad amplifier readout, 2x2 binning mode with rotating SDSS g , r and i filters. The integration time on target for each 1I frame was 180 sec, and 71 frames were acquired between 58055.1875 and 58055.3611 MJD. Bias frames were taken immediately before observing the target, and instrument flat fields were obtained on the sky at the end of the night. Absolute calibration was obtained using nearby SDSS flux calibrators in the 1I field. A similar observing strategy was used for the distant cometary nucleus survey of (Fernandez et al. 2016).

The weather was photometric throughout the night, and the seeing remained between 1.3” to 1.5”. Owing to 1I’s hyperbolic orbit, the object was fading rapidly in brightness after its discovery on 2017 October 18 and was observed as soon as possible with APO Director’s Discretionary time while 1I was within ~ 0.5 au of the Earth. The observing circumstances were not ideal (air mass = 1.3 to 2.0, 60% illuminated moon within 75° of 1I), but good measurements of 1I could still be obtained.

We used non-sidereal guiding matched to the rate of 1I’s motion to maximize our sensitivity to the target, which caused the background stars to trail by $\sim 10''$ in each image (Fig. 1). The motion of 1I on the sky fortuitously avoided significant overlap with the star trails, and its position within the frame was arranged to avoid cosmetic defects on the chip. The ARCTIC fields centered on the sky position of 1I contained a sufficient number of bright SDSS standard stars to enable accurate absolute calibration, despite the trailing of the stars.

3. THE COLORS OF 1I/‘OUMUAMUA

The position of 1I/‘Oumuamua in our field, and the input rates used to track the object, were nearly spot-on, despite its very high apparent angular rate of motion ($3'/h$) implying that the ephemeris solution we used was very good, and our results are consistent with an object on a hyperbolic interstellar orbit with eccentricity = 1.19. We did report astrometric details of our observations to the Minor Planet Center to help refine the orbit further (Weaver et al. 2017).

To measure colors, individual frames in our data set were bias subtracted and flat-fielded before being stacked in a robust average. Statistical outliers were removed at the 2σ level from the average stack of frames. The frames were stacked in two sets with one set centered on the motion of 1I and the other set stacked sidereally. All 15 g frames were stacked to create combined 1I and star centered images with an equivalent exposure time of 2700 s. All 6 i were stacked into a single exposure with the equivalent of a 1080 s of exposure time. Only 15 r frames were stacked for the purpose of comparing the photometry of the r band 1I detection with the g and i band detections. The 15 g , 15 r and 6 i were taken between 4.6 and 6.5 UTC, so they should have covered the same part of the rotation phase of 1I eliminating any differences in brightness between the color detections due to rotational change in brightness. Between 6.5 UTC to 8.6 UTC, only r exposures were taken. 1I was brightening during this time, so frames were stacked in shorter sequences of 2-6, as appropriate to reach a SNR $\gtrsim 10$.

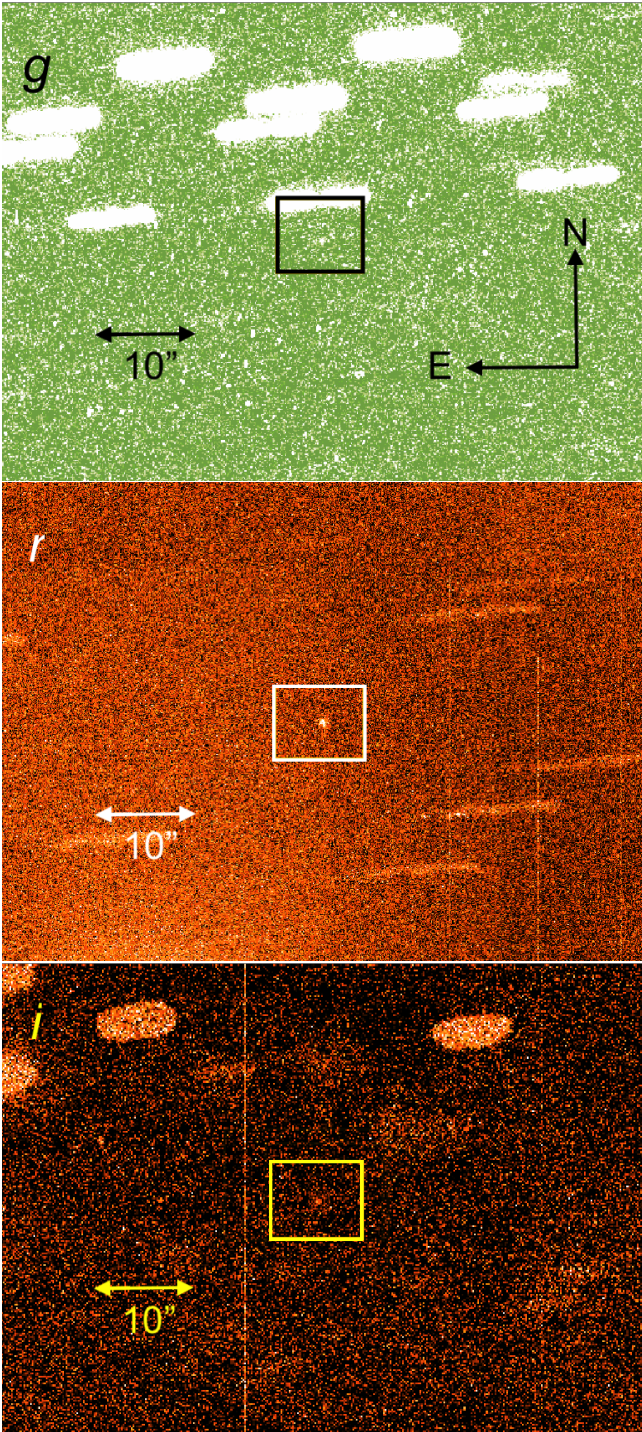


Figure 1. Mosaic of g , r and i images. The top panel is a robust average stack of 15 180 s g exposures. The center and bottom frames are robust average stacks of 6 180 s exposures in the r and i filters respectively. Outliers more than 2σ from the median are excluded from the stack. Artifacts (e.g., star trails, cosmic rays, a bad CCD column) are present, but none are within ~ 20 pixels of 11.

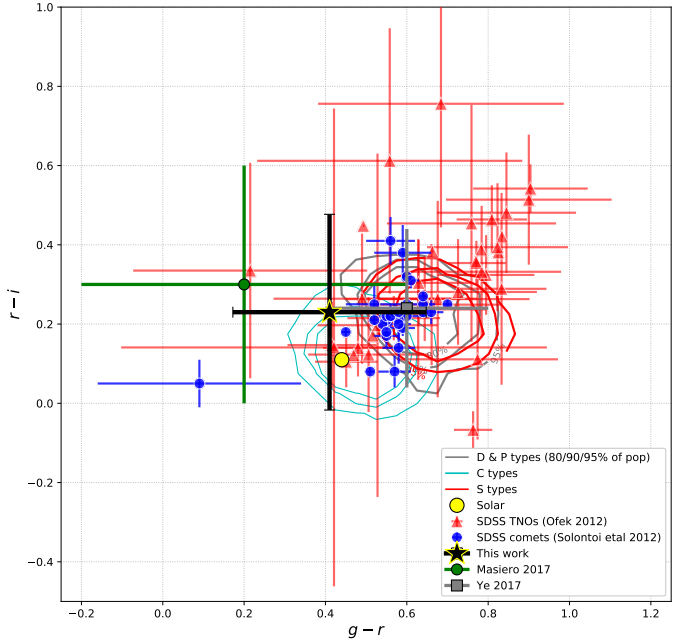


Figure 2. Measured $g-r$ vs. $r-i$ colors of 11/' Oumuamua in context with moving objects observed with SDSS (Ivezić et al. 2001; Jurić et al. 2002). Colors derived from detections in the SDSS Moving Object Catalog (MOC) (Ivezić et al. 2002) with a corresponding D or P, S, or C Bus-DeMeo taxonomic classification (DeMeo & Carry 2013) and $g-r$ and $r-i$ photometric errors smaller than 0.1 magnitudes are shown in the background contours; the illustrated contour intervals enclose 80, 90 and 95% of the objects in each class. TransNeptunian Objects (TNOs) generally move too slowly to be identified in the MOC, however Ofek (2012) cross-matched orbits of known (at the time) TNOs with reported photometry from SDSS Data Release 7. Colors of these objects are shown, with photometric errors, as red triangles. Comets also do not show up in the SDSS MOC, but Solontoi et al. (2012) searched for comets in SDSS catalogs using cuts on the catalogs directly and by cross-matching against known objects. Colors and photometric error bars of the resulting sample are shown with blue circles; note that these points likely refer to the color of the coma dust, not the nuclei. Our measured $g-r$ and $r-i$ colors and photometric errors of 11 are shown by the black star; colors from Masiero (2017) and Ye et al. (2017) are included as a green circle and gray square, respectively. While the error bars are large, 11's colors appear to be more consistent with those of C or D type asteroids than with the generally much redder colors of TNOs.

Aperture photometry was applied to the detections in the g , r and i frames. In most frames, an aperture radius of 5 pixels with a sky annulus between 15 and 20 pixel was used to measure the flux. An aperture radius of 30 pixels and a sky annulus between 40 and 45 pixels was used for the standard stars. The median sky background in the sky annulus was subtracted from the aperture flux in both the non-sidereally and sidereally stacked frames to minimize the potential effect of artifacts on the photometry.

The SDSS solar analogue star located at $RA\ 23:48:32.355$, $\delta\ +05:11:37.45$ with $g = 16.86$, $r = 16.41$ and $i = 16.22$ was used to calibrate the photometry in the g and i average stacks, and the average stack corresponding to the first 36 r frames. Following the 36th r frame, additional SDSS catalogue standard stars were used as the telescope’s tracking of 1I took it out of the frame of the imager. g , r and i magnitudes were measured at the $\gtrsim 5$ h level:

$$\begin{aligned} g &= 23.5 \pm 0.2 \\ r &= 23.1 \pm 0.1 \\ i &= 22.9 \pm 0.2 \end{aligned}$$

The photometric uncertainties are dominated by statistical noise because the effect of changing rotational brightness should have been averaged out as the exposures in the different bands were taken at the same time. The catalog magnitude uncertainty for the magnitude ~ 16.5 SDSS standard stars is within 0.01 magnitudes. The topocentric distance change was negligible over the course of the observations.

Our measured colors,

$$\begin{aligned} g - r &= 0.4 \pm 0.2 \\ r - i &= 0.2 \pm .3 \end{aligned}$$

are consistent with reported colors and Palomar and William Herschel Telescope optical spectra from Masiero (2017), Fitzsimmons et al. (2017) and Ye et al. (2017). When compared to the visible light colors of known objects in our Solar System (see Fig. 2), 1I’s colors are consistent with those of the rocky small bodies in our Solar System including solar colors, and are significantly less red than most Transneptunian Objects (TNOs), especially the cold classical TNOs.

The majority of r band detections in image stacks used in the light curve have an uncertainty of <0.1 , as seen in the top left panel of Fig. 3.

4. THE LIGHT CURVE OF 1I/‘OUMUAMUA

The data obtained in this paper do not allow for an unambiguous measurement of 1I’s light curve amplitude

and periodicity . We therefore add to our dataset the measurements reported by Knight et al. (2017) (henceforth referred to as the ‘DCT dataset’). Expected secular changes in magnitude due to changes in the distance from the Earth, Sun, and phase angle were removed prior to fitting the data. The combined data set is shown in Fig. 3.

Even with the extended dataset, estimating the light-curve period using the Lomb-Scargle periodogram (Lomb 1976; Scargle 1982) was inconclusive due to the sparse sampling pattern and the short time baseline of observations. This motivated us to apply more sophisticated methods – a direct Bayesian approach to model the observed light curve and estimate the period and amplitude of the periodic variation.

4.1. Simple Sinusoidal Model

We begin by modeling the light curve with a simple sinusoidal signal of the form:

$$\lambda_i = A \sin(2\pi t_i/P + \phi) + b, \quad (1)$$

where λ_i is the model magnitude at time step t_i , A , P and ϕ are the amplitude, period and phase of the sinusoid, respectively, and b denotes the constant mean of the light curve. This sinusoidal model is equivalent in concept to the generalized Lomb-Scargle (LS) periodogram (Lomb 1976; Scargle 1982), but the difference is that the LS periodogram assumes a well-sampled lightcurve, which cannot be guaranteed here. For details, see Ivezić et al. 2014. We model the data using a Gaussian likelihood and choose a flat prior on the period between 1 and 24 h, consistent with periods observed from similar sources known in the Solar System (Pravec et al. 2002).

Similarly, we choose a flat prior for b between 20 and 25 magnitudes, and an exponential prior for the logarithm of the amplitude between -20 and 20 . For the phase ϕ , we use a Von Mises distribution as appropriate for angles in order to incorporate the phase-wrapping in the parameters correctly, with a scale parameter $\kappa = 0.1$ and a mean of $\mu = 0$, corresponding to a fairly weak prior.

We sampled the posterior distribution of the parameters using Markov Chain Monte Carlo (MCMC), as implemented in the *Python* package *emcee* (Foreman-Mackey et al. 2013). This analysis reveals well-constrained, nearly Gaussian distributions for all relevant parameters. We summarize the marginalized posterior distributions in terms of their posterior means, as well as the 0.16 and 0.84 percentiles, corresponding to 1σ credible intervals. These are given by:

$$P_{\text{sin model}} = 4.07 \pm 0.01 \text{ hours}$$

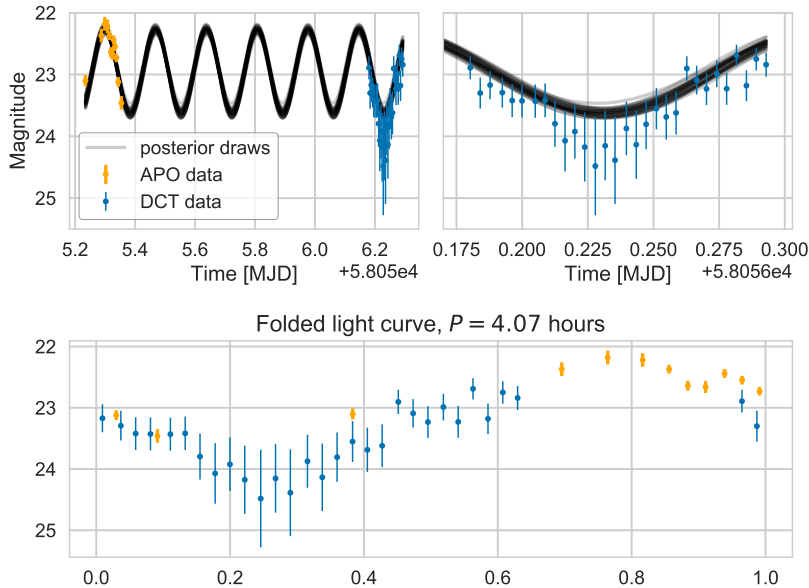


Figure 3. Sinusoidal model: APO data points (orange) and DCT data points (blue) as well as random samples from the posterior distribution for the parameters (grey). On the left, both data sets are plotted; the right panel contains a zoom into the DCT data set in order to show the variance in sine amplitudes and periods. The right panel also shows that the strictly sinusoidal model has difficulties exactly representing the data at the peak, indicating that this model might be too simplistic. The bottom panel shows the lightcurve folded at a 4 h period.

$$A_{\text{sin model}} = 0.64 \pm 0.05 \text{ mag}$$

for the period and the amplitude, respectively.

In Fig. 3, we show the observed light curve along with models drawn from the posterior distribution of the parameters. In particular, we show that the sinusoidal model slightly underestimates the minimum brightness in the DCT data set as seen in the right panel of Fig. 3. This is likely due to deviations from the sinusoidal shape, which compels the model to adequately fit the wings rather than the peak.

4.2. Gaussian Process Model

Figure 3 indicates that the strictly sinusoidal model is too simplistic to adequately model the more complex light curve shape of the object. We therefore turn to a more complex model that, while still periodic, allows for non-sinusoidal as well as double-peaked light curve shapes. In short, instead of modelling the light curve directly as above, we model the *covariance* between data points, a method commonly referred to as Gaussian Processes (GPs; see Rasmussen & Williams 2006 for a pedagogical introduction). This approach has recently been

successfully deployed in a range of astronomical applications (e.g., Angus et al. 2017; Jones et al. 2017). The covariance matrix between data points is modelled by a so-called covariance function or kernel. Different choices are appropriate for different applications, and we choose a strictly periodic kernel of the following form (MacKay 1998) here:

$$k(t_i, t_j) = C \exp\left(\frac{\sin^2(\pi|t_i - t_j|/P)}{d^2}\right) \quad (2)$$

for time stamps t_i and t_j . In this framework, the amplitude C corresponds to the amplitude of the covariance between data points and is thus not comparable to the amplitude in the sinusoidal model above. The period P on the other hand retains exactly the same meaning. The model also gains an additional parameter d describing the length scale of variations within a single period. It is defined with respect to the period, with $d \gg P$ leading to sinusoidal variations, whereas increasingly smaller values result in an increasingly complex harmonic content within each period.

We use a Gaussian Process, as implemented in the Python package *george* (Ambikasaran et al. 2014), with the covariance function defined above, to model the combined DCT and APO data sets. For the period, we use the same prior as for the sinusoidal model, but we assume uniform priors on the logarithms of amplitude ($-100 < \log(C) < 100$) and the length scale of within-period variations, $\Gamma = 1/d^2$ ($-20 < \log(\Gamma) < 20$). As before, we use *emcee* to draw MCMC samples from the posterior probability. In Fig. 4, we show the posterior distributions for the period, amplitude and Γ parameter. The marginalized posterior probability distribution for the period is in broad agreement with the sinusoidal model at $P = 4.07$ h.

We inferred what the expected light curve profile would look like if the period were twice that inferred by both the sinusoidal and Gaussian Process model in order to guide additional observations of 11/‘Oumuamua, either with improved photometry from existing observations or future observations before the object becomes too faint as it leaves the Solar System. We took the parameters with the highest posterior probability, doubled its period, and computed the 1σ credible intervals for the model light curve admitted by this particular Gaussian Process with these parameters (Fig. 4, lower panel). This figure shows that if a double-peaked profile were present, roughly half of it would be well-constrained by current observations (indicated by narrow credible intervals). The second peak of the profile, however, is considerably less well constrained due to the lack of data points. Observations in that part of phase space, in par-

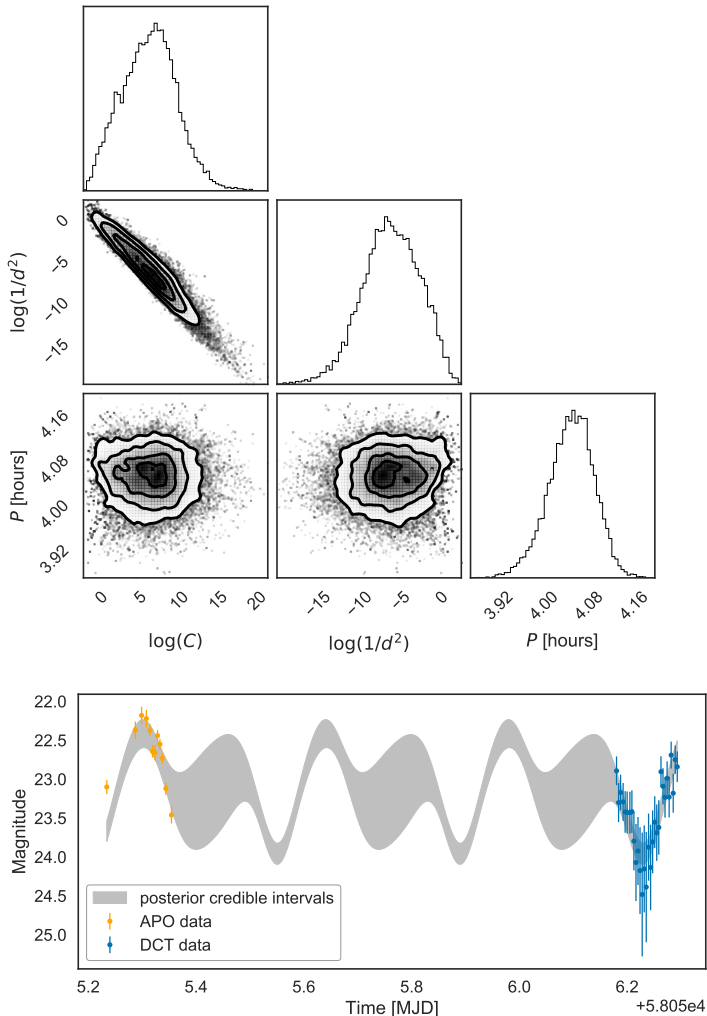


Figure 4. First panel: corner plot (Foreman-Mackey 2016) of the parameter inference done with *emcee* on the Gaussian Process model. The period shows several distinct modes, with most of the probability concentrated around 4 h. Second panel: the APO and DCT superimposed in orange and blue with a Gaussian process model with twice the period of the highest mode in the posterior (blue). The banded intervals present the 1σ confidence intervals of the possible function space allowed by the Gaussian Process. It is narrow where data points tightly constrain the possible models, but wider where no data exists to constrain a possible second peak in the lightcurve profile.

ticular near the minimum and maximum of that second peak, could help pin down the exact light curve shape.

5. RESULTS AND DISCUSSION

1I was challenging to characterize with the Apache Point Observatory due to its faintness. Initially, while observing, it was impossible to find the object in our standard 180 s integrations, but as the night progressed

it became distinct, indicating a significant brightening in less than 4 h. A similar behavior was reported by Knight et al. (2017) in observations from the DCT 4m on the next night (Fig 2). Combining the two datasets, we find a most likely lightcurve period period of 4.07 h as described in Section 4; phasing the data to this period produces a well structured, near-sinusoidal lightcurve as seen in the bottom panel of Fig. 3. The max-to-min amplitude of the lightcurve, almost 2 magnitudes, is unusual compared to the population of asteroids in the Solar System, which usually have peak-to-peak amplitudes of <0.75 (Warner et al. 2009).

We estimate the size of 1I from a clean set of 4 r band photometric images taken in the middle of our run, when the telescope pointing and focus had stabilized. Using the 15.23 r magnitude reference star, UCAC4 ID 477-131394 with 4.08×10^6 DN sky-subtracted counts, we find our 2.42×10^3 DN sky-subtracted counts from 1I in 180 s translates into a 22.41 r magnitude object at a heliocentric distance of 1.458 au and geocentric distance of 0.534 au. Assuming the r band zero-point to be 3.631×10^3 Jy, this yields an in-band flux density of 3.03×10^{-17} $\text{W m}^{-2} \mu\text{m}^{-1}$. Using a solar flux density of 1.90×10^3 $\text{W m}^{-2} \mu\text{m}^{-1}$ at the r band central wavelength of $0.624 \mu\text{m}$, we find an effective radius of 0.120 km assuming a surface scattering albedo of 0.10, or an effective radius of 0.200 km for a surface albedo of 0.04 (both quoted albedos refer to the values at a solar phase angle of 24°).

The size and shape of 1I’s image was consistent with a point source throughout the observing run, with no evidence for an extended source even in a stacked image of all the APO r band data. This is unlike many of our distant comet program targets (Fernandez et al. 2016), which we have over 10 years worth of experience observing for size, rotation rate, and signs of activity. The object was well-detected in multiple 180 s r band images, but it took all of our 15 g band 180 s exposures and all 6 of our i band 180 s exposures to obtain a detection at $\text{SNR} \sim 5$. As discussed above and shown in Fig. 1, the colors of 1I are consistent with the apparently inactive, asteroidal nature of the object.

We used the 1I ephemeris from the JPL Horizons system (reference solution #4) to drive the APO telescope pointing and tracking, the latter at the relatively high rate of $\sim 3' \text{h}^{-1}$. The location of 1I in our field, and the essentially point source appearance of 1I even after stacking multiple images, provided strong evidence that 1I’s orbital elements were accurate and thus consistent with an interstellar origin for the object. We reported astrometric details of our observations to the

Minor Planet Center to help refine the orbit further (Weaver et al. 2017).

The peak-to-peak amplitude of our lightcurve, determined by the difference between the minimum and maximum brightness (Barucci & Fulchignoni 1982) of 11, is $A_{\text{peak,difference}} = 2.05 \pm 0.53$ as seen in Fig. 3. $A_{\text{peak,sin model}} = 2A_{\text{sin model}} = 1.28 \pm 0.1$ mag.

The angle between the observer and the sun from the point of view of the asteroid, or the phase angle, α , can affect the measured lightcurve peak-to-peak amplitude. (Zappalà et al. 1990) found that the peak-to-peak amplitudes increase with the phase angle, α according to

$$\Delta m(\alpha = 0^\circ) = \frac{\Delta m(\alpha)}{1 + s\alpha} \quad (3)$$

where s is the slope of the increase in peak-to-peak magnitude with α . (Zappalà et al. 1990) and Gutiérrez et al. (2006) found that s varies with taxonomic type and with asteroid surface topography. We adopt a value of $0.015 \text{ mag deg}^{-1}$ as an average value of s (Zappalà et al. 1990). α at the time of the APO and DCT observations 11 was 24° which according to Eq 3 corrects $A_{\text{peak,difference}}$ and $A_{\text{peak,sin model}}$ by a factor of 0.73, so that $A_{\text{peak,difference}} \simeq 1.51$ and $A_{\text{peak,sin model}} \simeq 0.94$.

Asteroids are assumed in the general case to have a simplistic triaxial shape with an axial ratio, $a:b:c$ where $a \geq b \geq c$ (Binzel et al. 1989). As a result, the aspect angle between the observer's line of sight and the rotational pole of the asteroid, θ , can modify the measured peak-to-peak amplitude as the rotational cross section with respect to the observer increases or decreases for different θ , a , b and c Barucci & Fulchignoni (1982); Thirouin et al. (2016). From (Thirouin et al. 2016), the difference in peak-to-peak magnitude observed at angle θ and peak-to-peak magnitude observed at angle $\theta = 90^\circ$ as a function of θ , a , b and c is

$$\Delta m(\theta) - \Delta m(\theta = 90^\circ) = 1.25 \log \left(\frac{a^2 \cos^2 \theta + c^2 \sin^2 \theta}{b^2 \cos^2 \theta + c^2 \sin^2 \theta} \right) \quad (4)$$

Assuming $b = c$, Eq. 4 implies that Δm will be ~ 0.6 magnitudes fainter on average compared $\Delta m(\theta = 90^\circ)$ with the assumptions that $2 < a/b < 4$ and $b = c$. We can estimate upper limits for the peak-to-peak magnitudes at $\theta = 90^\circ$ by re-calculating $A_{\text{peak,difference}}$ and $A_{\text{peak,sin model}}$ with the assumption that the data used for their calculations are representative of the average aspect angle and have $2 < a/b < 4$ and $b = c$ by using Eq. 4

$$A_{\text{max,difference}} = A_{\text{peak,difference}} - \Delta m(\theta = 90^\circ)$$

$$A_{\text{max,sin model}} = A_{\text{peak,sin model}} - \Delta m(\theta = 90^\circ)$$

results in $A_{\text{max,difference}} = 2.11 \pm 0.53$ and $A_{\text{max,sin model}} = 1.54 \pm 0.1$.

Assuming 11 is a triaxial body with an axial ratio $a:b:c$ where $a \geq b \geq c$ and that the lightcurve variation in magnitude is wholly due to the changing projected surface area (consistent with the sinusoidal shape of our phased lightcurve), we obtain an upper limit of $a/b = 6.91 \pm 3.41$ from $a/b = 10^{0.4\Delta M}$ (Binzel et al. 1989) where $\Delta M = A_{\text{max,difference}}$. A more conservative estimate of the upper limit on the peak-to-peak amplitude is given by using $A_{\text{max,sin model}}$ for ΔM resulting in $a/b = 4.13 \pm 0.48$. The uncertainty in the $a/b = 6.98 \pm 3.41$ using $\Delta M = A_{\text{peak,difference}}$ is dominated by uncertainty on magnitude measurement compared to $A_{\text{max,sin model}}$. The uncertainty of $A_{\text{max,sin model}}$ are determined by the spread of compatible values for the amplitude within the uncertainties of all data points in the lightcurve and probably more statistically robust than using the difference between the minimum and maximum brightness data points in the lightcurve. However, this fact must be tempered by the fact that the true peak-to-peak amplitude may be underestimated due to the sparseness of data points as described in Section 4. Therefore, we assume that the true axial ratio a/b lies between $4.13 \lesssim a/b \lesssim 6.91$. These limits are based generalized assumptions and more accurately determining the true value of a/b would require additional observations at different θ and at times in which the object's rotation are not covered by our observations as discussed in Section 4.2.

This large value for $A_{\text{peak,difference}}$ or $A_{\text{peak,sin model}}$ suggests that the modulation seen in the lightcurve is due to the rotation of an elongated triaxial body dominated by the second harmonic resulting in a bimodal, double-peaked lightcurve (Harris et al. 2014; Butkiewicz-Bąk et al. 2017). Thus, we obtain a double-peaked amplitude of $P_{\text{rotation}} = 2P_{\text{sin model}}$ or 8.14 ± 0.02 h. Non-triaxial asteroid shapes can result in lightcurves exceeding two peaks per rotation period, but this case is ruled out as unlikely case given because the large amplitude of the lightcurve strongly favors an elongated object (Harris et al. 2014). Another alternative explanation of the rotation period is that the lightcurve variation is due to surface variations in the reflectivity of the asteroid. Surface variations result in single-peaked lightcurves (Barucci et al. 1989), but the similarity of the colors and spectra of 11 obtained in observations taken at different times (Masiero 2017; Fitzsimmons et al. 2017; Ye et al. 2017) does not suggest significant variation on the object's surface.

Asteroid elongations with $4.0 \lesssim a/b \lesssim 7.0$ are uncommon for asteroids in the Solar System where the majority of have $a/b < 2.0$ (Cibulková et al. 2016, 2017). Smaller asteroids have been observed to have statistically higher

elongations than larger asteroids (Pravec et al. 2008; Cibulková et al. 2016). Smaller asteroids and comets have weaker gravity and may be under structural stress due to stress imposed by their rotation possibly resulting in plasticity of their structure (Harris et al. 2009; Hirabayashi & Scheeres 2014; Hirabayashi 2015) or may become reconfigured after fracturing due to rotational stress (Hirabayashi et al. 2016).

To examine the possibility that rotational stress might be an explanation for the large elongation of 1I/‘Oumuamua, we must examine the existing evidence for rotational breakup of asteroids in the Solar System. Asteroids in the Solar System have been observed to undergo rotational break up into fragments such as active asteroids spin-up by thermal recoil forces (Rubincam 2000; Jewitt et al. 2015b). Additionally, active comets and asteroids can become spun up due to the sublimation of volatiles (Samarasinha & Mueller 2013; Steckloff & Jacobson 2016).

The critical breakup period for a strengthless rotating ellipsoid with an axial ratio is given by (Samarasinha et al. 2004; Jewitt et al. 2015b)

$$P_{critical\ period} = \left[(a/b) \left(\frac{3\pi}{G\rho} \right) \right]^{1/2} \quad (5)$$

where ρ is the asteroid density. Fig. 5 shows the value of $P_{critical\ period}$ in h for values of a/b allowable by our results and ρ for different Solar System asteroid taxonomic types from comets, D-types with 0.5-1.0 g cm^{-3} , B and C-types with 1.2-1.4 g cm^{-3} , S-types with 2.3 g cm^{-3} , X-types with 2.7 g cm^{-3} , rubble piles with 3.3 g cm^{-3} and 4 g cm^{-3} for M-types (Lisse et al. 1999; Britt et al. 2002; A’Hearn et al. 2005; Fujiwara et al. 2006; Carry 2012).

As seen in Fig. 5, the observed ~ 8 h rotational period of 1I is much longer than the critical break up period described by most of the a/b vs. ρ phase space covering most common asteroid densities for $4.0 \lesssim a/b \lesssim 7.0$ as seen in Fig. 5. 1I would have to have $0.9 \text{ g cm}^{-3} < \rho < 1.5 \text{ g cm}^{-3}$ for $4.0 < a/b < 7.0$ to be rotating near its breakup limit with a period of 8 h. C type asteroids and comets have densities this low, so it is not impossible for 1I to be rotating near its strengthless breakup limit if it is similar in ρ to C type asteroids and comets.

One possibility if 1I is rotating near its breakup limit is that it may be shedding material visible as a coma. Asteroids have been observed in the Solar System by their activity as a result of rotational breakup for P/2013 P5 and P/2013 R3 (Bolin et al. 2013; Hill et al. 2013; Jewitt et al. 2015a, 2017). However deep stacking of detections of 1I in our own r images as well as images of others have revealed no detectable presence of a coma

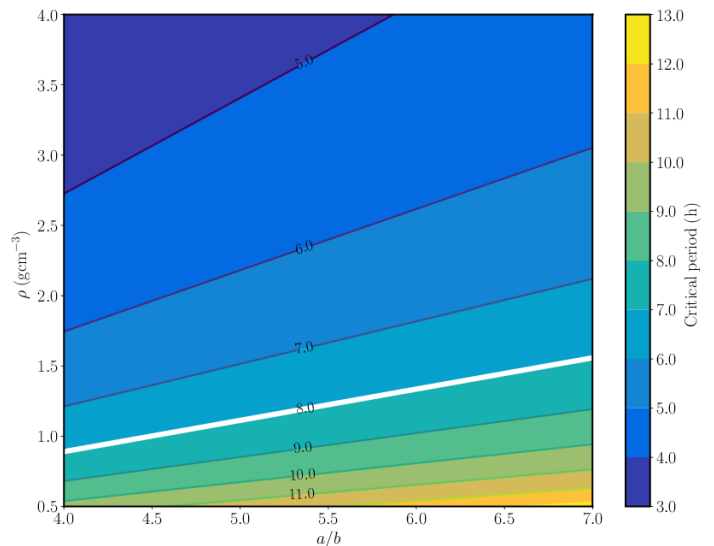


Figure 5. The critical period described by Eq. 5 as a function of a/b and ρ assuming zero cohesive strength. The contour for a critical period of 8 is plotted in white.

(Knight et al. 2017; Williams 2017). This suggests that 1I is rotating slower than its rotational breakup limit and its critical period must be >8 h, greater than the period that we measure for its rotation.

1I/‘Oumuamua’s structure may have cohesive strength keeping it from disrupting or shedding material that would be detectable as a coma. Under the assumption that the 8 h rotation period is near the critical breakup limit described by Eq. 5 combined with a high axial ratio and $\lesssim 1 \text{ g cm}^{-3}$ ρ , 1I may have some internal cohesive strength keeping it from disrupting as observed for other small bodies in the Solar System (Lisse et al. 1999; Rozitis & Green 2014; ?). However, assuming the force per unit area on the surface of a body is given by $2\pi^2\rho P^{-2}r^2$ (Lisse et al. 1999), the minimum cohesive force required to stabilize an $r = 0.15 \text{ km}$, $\rho = 1 \text{ g cm}^{-3}$ object spinning with 8.14 h period is only 0.5 Pa, well below even the 10 Pa bulk cohesive strength of extremely weak materials like talcum powder or beach sand held together mainly by inter-grain friction (Sánchez & Scheeres 2014). Thus even a real rubble pile, influenced by inter-block frictional forces, could be stable from our measurements. The implication is that either 1I has either both a lower ρ than we are considering and a moderate cohesive strength, or it has a $\rho \gtrsim 1 \text{ g cm}^{-3}$ to keep from rotationally disrupting in the regime where cohesive strength is irrelevant.

6. CONCLUSION

We observed interstellar asteroidal object 11/'Oumuamua from the Apache Point Observatory on 29 Oct 2017 from 04:28 to 08:40 UTC. 3-color photometry and time domain observations were obtained in the g , r and i bands down to magnitudes of 22 to 23. An unresolved object with solar, or slightly reddish, color and variable brightness was found. The results from our observations are consistent with the point source nature and slightly reddish color found by other observers. The asteroidal-like appearance and nearly solar-like color of 11 suggests formation in a volatile-poor region near its parent star, rather than in an icy-rich exoplanetary region.

Combining APO and DCT time domain photometry, we found that 11 was rotating with a period of ~ 8.14 hrs, which is consistent with the rotational periods of many Solar System asteroids (Warner et al. 2009). We also found that 11's light curve amplitude was ~ 1.5 -2 mag, suggesting an axial ratio of $a:b \sim 4:1$ -7:1. Our results on the light curve period and amplitude are compatible with 11 having a density > 1.0 g cm $^{-3}$, or having modest cohesive strength. Our modeling of the light curve data with Gaussian processing shows when during 11's rotation phase additional observations can be used to improve constraints on the period and axial ratio.

The apparent large axial ratio of 11 seems to not be originated by rotational disruption as indicated by its present ~ 8 h rotation period although it has been shown that asteroids can have plasticity in their structure due to rotational stress without undergoing disrupting such as can be for the case of asteroid Cleopatra (Hirabayashi & Scheeres 2014). Thermal recoil forces such as the Yarkovsky-O'Keefe-Radzievskii-Paddack effect (YORP) (Rubincam 2000; Bottke et al. 2006; Vokrouhlický et al. 2015) could have modified its rotation rate to structurally altering or disruptive rotation periods while 11 was in its home system. However the object would have gone through YORP cycles resulting in its spin period being slowed down to the value we see today (Čapek & Vokrouhlický 2004). This YORP cycle induced slow-down would have had to occur while 11 was still close to its host star. YORP modification of an asteroid's spin rate is thermally dependent and has a greater affect on asteroids that are closer to the sun and non-effective at heliocentric distances exceeding 10 au for 100 m scale asteroids (Vokrouhlický et al. 2006, 2007). Therefore, if the 11 did have a faster spin period at one time, it would have been before it left its home system. Perhaps the fact that 11 has a shape potentially originated by YORP and later had its spin period slowed down is additional evidence when combined with colors and spectra that 11 could not have originated from too far from its host star

before it was ejected from its star system before reaching ours.

Another explanation for the elongated shape of 11 is that it obtained its elongated shape when it was ejected from its home system during a close encounter with a planet or a star. It is known that asteroids and comets can be ejected from the solar system during close encounters with planets (Granvik et al. 2017). During these close encounters, objects can pass within the Roche limit the planet subjecting their structure to tidal forces. We can eliminate the possibility that 11 experienced tidal disruption during its passage through the solar system because it came no more within 10 times the Roche limit distance from the sun during its perihelion passage on 2017 November 09.

It has been shown that tidal forces can completely disrupt the structure of comets and asteroids such as in the complete disruption of Comet Shoemaker-Levy 9 during its close encounter with Jupiter (Shoemaker 1995; Asphaug & Benz 1996) and the partial disruption of the asteroid Geographos during close encounters with the Earth (Bottke et al. 1999; Durech et al. 2008; Rozitis & Green 2014). Modeling of asteroids and comets under the stress of tidal forces reveals that one result of tidal disruption is that their structures become elongated due to the stress of tidal forces (Solem & Hills 1996; Richardson et al. 1998; Walsh & Jacobson 2015). Furthermore, in the complete disruption case of an asteroid or comet by tidal disruption, the fragmentation of the parent body can result in fragments having elongated shapes (Walsh & Richardson 2006; Richardson et al. 2009). Therefore, 11 could have attained its elongated structure while experiencing tidal disruption itself, or while being produced as a fragment from a larger body undergoing complete tidal disruption.

We can set a rough upper limit to the density of 11 if we assume that it had to have been shaped by tidal forces as a result of a close encounter with a gas giant planet by using the scaling for tidal disruption distance of a brittle or cohesionless body from Dobrovolskis (1990)

$$1 < \frac{d}{R} < 1.37 \left(\frac{\rho_{11}}{\rho_{planet}} \right)^{-1/3} \quad (6)$$

where d and R are the close passage distance and planet radius. Using the above limit and assuming $\rho_{planet} = 1.33$ g cm $^{-3}$, the density of Jupiter (Simon et al. 1994), we obtain a maximum density of 3.41 g cm $^{-3}$ for $\frac{d}{R} \gtrsim 1$ which is a realistic assumption comparable to S or C type asteroids in the solar system (Carry 2012). If 11 has a density greater than 3.41 g cm $^{-3}$ or considerable cohesive strength would be less prone to tidal disruption

and some other mechanism would have to be used to explain its extreme elongation.

ACKNOWLEDGMENTS

We thank the APO Director (Nancy Chanover) and Deputy Director (Ben Williams) for their enthusiastic and timely support of our Director’s Discretionary Time (DDT) proposals. We also thank Russet McMillan and the rest of the APO technical staff for their assistance in performing the observations just two days after our DDT proposals were submitted. We thank Ed Lu, Sarah Tuttle, and Ben Weaver for fruitful discussions and advice that made this paper possible. BTB would like to acknowledge the generous support of the B612 Foundation’s Asteroid Institute. MJ and CTS wish to acknowledge the support of the Washington Research Foundation Data Science Term Chair fund and the University of Washington Provost’s Initiative in Data-Intensive Discovery. BTB, DH, RLJ, MJ, JM, MLG, CTS, ECB and AJC wish to acknowledge the support of DIRAC (Data Intensive Research in Astronomy and Cosmology) Institute at the University of Washington. Joachim Moeyens thanks the LSSTC Data Science Fellowship Program, his time as a Fellow has benefited this work.

We would also like to thank Marco Delbó, Alan Fitzsimmons, Robert Jedicke and Alessandro Morbidelli for constructive feedback and discussion when planning this project.

Funding for the creation and distribution of the SDSS Archive has been provided by the Alfred P. Sloan Foundation, the Participating Institutions, the National Aeronautics and Space Administration, the National Science Foundation, the U.S. Department of Energy, the Japanese Monbukagakusho, and the Max Planck Society. The SDSS Web site is <http://www.sdss.org/>.

The SDSS is managed by the Astrophysical Research Consortium (ARC) for the Participating Institutions. The Participating Institutions are The University of Chicago, Fermilab, the Institute for Advanced Study, the Japan Participation Group, The Johns Hopkins University, the Korean Scientist Group, Los Alamos National Laboratory, the Max-Planck-Institute for Astronomy (MPIA), the Max-Planck-Institute for Astrophysics (MPA), New Mexico State University, University of Pittsburgh, University of Portsmouth, Princeton University, the United States Naval Observatory, and the University of Washington.

Software: *Astropy* (Astropy Collaboration et al. 2013), *emcee* (Foreman-Mackey et al. 2013)

REFERENCES

- A’Hearn, M. F., Belton, M. J. S., Delamere, W. A., et al. 2005, *Science*, 310, 258
- Ambikasaran, S., Foreman-Mackey, D., Greengard, L., Hogg, D. W., & O’Neil, M. 2014
- Angus, R., Morton, T., Aigrain, S., Foreman-Mackey, D., & Rajpaul, V. 2017, ArXiv e-prints, arXiv:1706.05459
- Asphaug, E., & Benz, W. 1996, *Icarus*, 121, 225
- Astropy Collaboration, Robitaille, T. P., Tollerud, E. J., et al. 2013, *A&A*, 558, A33
- Barucci, M. A., Capria, M. T., Harris, A. W., & Fulchignoni, M. 1989, *Icarus*, 78, 311
- Barucci, M. A., & Fulchignoni, M. 1982, *Moon and Planets*, 27, 47
- Binzel, R. P., Farinella, P., Zappalà, V., & Cellino, A. 1989, in *Asteroids II*, ed. R. P. Binzel, T. Gehrels, & M. S. Matthews, 416–441
- Bolin, B., Denneau, L., Micheli, M., et al. 2013, *Central Bureau Electronic Telegrams*, 3639
- Bottke, Jr., W. F., Richardson, D. C., Michel, P., & Love, S. G. 1999, *AJ*, 117, 1921
- Bottke, Jr., W. F., Vokrouhlický, D., Rubincam, D. P., & Nesvorný, D. 2006, *Annual Review of Earth and Planetary Sciences*, 34, 157
- Britt, D. T., Yeomans, D., Housen, K., & Consolmagno, G. 2002, *Asteroids III*, 485
- Butkiewicz-Bąk, M., Kwiatkowski, T., Bartczak, P., Dudziński, G., & Marciniak, A. 2017, *MNRAS*, 470, 1314
- Carry, B. 2012, *Planet. Space Sci.*, 73, 98
- Cibulková, H., Ďurech, J., Vokrouhlický, D., Kaasalainen, M., & Oszkiewicz, D. A. 2016, *A&A*, 596, A57
- Cibulková, H., Nortunen, H., Ďurech, J., et al. 2017, ArXiv e-prints, arXiv:1709.05640
- Cook, N. V., Ragozzine, D., Granvik, M., & Stephens, D. C. 2016, *ApJ*, 825, 51
- DeMeo, F. E., & Carry, B. 2013, *Icarus*, 226, 723
- Dobrovolskis, A. R. 1990, *Icarus*, 88, 24
- Durech, J., Vokrouhlický, D., Kaasalainen, M., et al. 2008, *A&A*, 489, L25
- Engelhardt, T., Jedicke, R., Vereš, P., et al. 2017, *AJ*, 153, 133
- Fernandez, Y. R., Weaver, H. A., Lisse, C. M., et al. 2016, in *American Astronomical Society Meeting Abstracts*, Vol. 227, American Astronomical Society Meeting Abstracts, 141.22
- Fitzsimmons, A., M., H., R., J., C., S., & B., Y. 2017, *Central Bureau Electronic Telegrams*

- Foreman-Mackey, D. 2016, *The Journal of Open Source Software*, 24, doi:10.21105/joss.00024
- Foreman-Mackey, D., Hogg, D. W., Lang, D., & Goodman, J. 2013, *PASP*, 125, 306
- Fujiwara, A., Kawaguchi, J., Yeomans, D. K., et al. 2006, *Science*, 312, 1330
- Granvik, M., Morbidelli, A., Vokrouhlický, D., et al. 2017, *A&A*, 598, A52
- Gutiérrez, P. J., Davidsson, B. J. R., Ortiz, J. L., Rodrigo, R., & Vidal-Nuñez, M. J. 2006, *A&A*, 454, 367
- Harris, A. W., Fahnestock, E. G., & Pravec, P. 2009, *Icarus*, 199, 310
- Harris, A. W., Pravec, P., Galád, A., et al. 2014, *Icarus*, 235, 55
- Hill, R. E., Veres, P., Bolin, B., et al. 2013, *Central Bureau Electronic Telegrams*, 3712
- Hirabayashi, M. 2015, *MNRAS*, 454, 2249
- Hirabayashi, M., & Scheeres, D. J. 2014, *ApJ*, 780, 160
- Hirabayashi, M., Scheeres, D. J., Chesley, S. R., et al. 2016, *Nature*, 534, 352
- Huehnerhoff, J., Ketzbeck, W., Bradley, A., et al. 2016, in *Proc. SPIE*, Vol. 9908, *Ground-based and Airborne Instrumentation for Astronomy VI*, 99085H
- Ivezić, Ž., Connolly, A. J., VanderPlas, J. T., & Gray, A. 2014, *Statistics, Data Mining, and Machine Learning in Astronomy: A Practical Python Guide for the Analysis of Survey Data* (Princeton University Press)
- Ivezić, Ž., Tabachnik, S., Rafikov, R., et al. 2001, *AJ*, 122, 2749
- Ivezić, Ž., Lupton, R. H., Jurić, M., et al. 2002, *AJ*, 124, 2943
- Jewitt, D., Agarwal, J., Li, J., et al. 2017, *AJ*, 153, 223
- Jewitt, D., Agarwal, J., Weaver, H., Mutchler, M., & Larson, S. 2015a, *ApJ*, 798, 109
- Jewitt, D., Hsieh, H., & Agarwal, J. 2015b, *The Active Asteroids*, ed. P. Michel, F. E. DeMeo, & W. F. Bottke, 221–241
- Jones, D. E., Stenning, D. C., Ford, E. B., et al. 2017, *ArXiv e-prints*, arXiv:1711.01318
- Jurić, M., Ivezić, Ž., Lupton, R. H., et al. 2002, *AJ*, 124, 1776
- Knight, M. M., Protopapa, S., Kelley, M. S. P., et al. 2017, *ArXiv e-prints*, arXiv:1711.01402
- Lisse, C. M., Beichman, C. A., Bryden, G., & Wyatt, M. C. 2007, *ApJ*, 658, 584
- Lisse, C. M., Sitko, M. L., Marengo, M., et al. 2017, *AJ*, 154, 182
- Lisse, C. M., Fernández, Y. R., Kundu, A., et al. 1999, *Icarus*, 140, 189
- Lomb, N. R. 1976, *Ap&SS*, 39, 447
- MacKay, D. J. 1998, *NATO ASI Series F Computer and Systems Sciences*, 168, 133
- Masiero, J. 2017, *ArXiv e-prints*, arXiv:1710.09977
- Nomura, H., Tsukagoshi, T., Kawabe, R., et al. 2016, *ApJL*, 819, L7
- Öberg, K. I., Guzmán, V. V., Furuya, K., et al. 2015, *Nature*, 520, 198
- Ofek, E. O. 2012, *The Astrophysical Journal*, 749, 10
- Pravec, P., Harris, A. W., & Michalowski, T. 2002, *Asteroid Rotations*, ed. W. F. Bottke, Jr., A. Cellino, P. Paolicchi, & R. P. Binzel, 113–122
- Pravec, P., Harris, A. W., Vokrouhlický, D., et al. 2008, *Icarus*, 197, 497
- Rasmussen, C. E., & Williams, C. K. 2006, *Gaussian processes for machine learning*, Vol. 1 (MIT press Cambridge)
- Richardson, D. C., Bottke, W. F., & Love, S. G. 1998, *Icarus*, 134, 47
- Richardson, D. C., Michel, P., Walsh, K. J., & Flynn, K. W. 2009, *Planet. Space Sci.*, 57, 183
- Rozitis, B., & Green, S. F. 2014, *A&A*, 568, A43
- Rubincam, D. P. 2000, *Icarus*, 148, 2
- Samarasinha, N. H., & Mueller, B. E. A. 2013, *ApJL*, 775, L10
- Samarasinha, N. H., Mueller, B. E. A., Belton, M. J. S., & Jorda, L. 2004, *Rotation of cometary nuclei*, ed. G. W. Kronk, 281–299
- Sánchez, P., & Scheeres, D. J. 2014, *Meteoritics and Planetary Science*, 49, 788
- Scargle, J. D. 1982, *ApJ*, 263, 835
- Shoemaker, E. M. 1995, *Geophys. Res. Lett.*, 22, 1555
- Simon, J. L., Bretagnon, P., Chapront, J., et al. 1994, *A&A*, 282, 663
- Solem, J. C., & Hills, J. G. 1996, *AJ*, 111, 1382
- Solontoi, M., Ivezić, Ž., Jurić, M., et al. 2012, *Icarus*, 218, 571
- Steckloff, J. K., & Jacobson, S. A. 2016, *Icarus*, 264, 160
- Thirouin, A., Moskovitz, N., Binzel, R. P., et al. 2016, *AJ*, 152, 163
- Čapek, D., & Vokrouhlický, D. 2004, *Icarus*, 172, 526
- Vokrouhlický, D., Bottke, W. F., Chesley, S. R., Scheeres, D. J., & Statler, T. S. 2015, *Asteroids IV*, 509
- Vokrouhlický, D., Breiter, S., Nesvorný, D., & Bottke, W. F. 2007, *Icarus*, 191, 636
- Vokrouhlický, D., Brož, M., Bottke, W. F., Nesvorný, D., & Morbidelli, A. 2006, *Icarus*, 182, 118
- Walsh, K. J., & Jacobson, S. A. 2015, *Formation and Evolution of Binary Asteroids*, ed. P. Michel, F. E. DeMeo, & W. F. Bottke, 375–393
- Walsh, K. J., & Richardson, D. C. 2006, *Icarus*, 180, 201

Warner, B. D., Harris, A. W., & Pravec, P. 2009, *Icarus*,
202, 134

Weaver, H. A., Bolin, B. T., Fernandez, Y. R., et al. 2017,
Minor Planet Electronic Circulars, 2017

Williams, G. V. 2017, Minor Planet Electronic Circulars

Ye, Q.-Z., Zhang, Q., Kelley, M. S. P., & Brown, P. G.
2017, ArXiv e-prints, arXiv:1711.02320

Zappalà, V., Cellino, A., Farinella, P., & Knežević, Z. 1990,
AJ, 100, 2030